# Improved SWMM Modeling for Rapid Pipe Filling Incorporating Air Behavior in Intermittent Water Supply Systems

Ferreira, João P.; Ferras, David; Covas, Dídia I.C.; Kapelan, Zoran

**DOI**
10.1061/JHEND8.HYENG-13137

**Publication date**
2023

**Document Version**
Final published version

**Published in**
Journal of Hydraulic Engineering

**Citation (APA)**
Ferreira, J. P., Ferras, D., Covas, D. I. C., & Kapelan, Z. (2023). Improved SWMM Modeling for Rapid Pipe Filling Incorporating Air Behavior in Intermittent Water Supply Systems. *Journal of Hydraulic Engineering*, *149*(4), Article 04023004. https://doi.org/10.1061/JHEND8.HYENG-13137

ASCE

# Improved SWMM Modeling for Rapid Pipe Filling Incorporating Air Behavior in Intermittent Water Supply Systems

João P. Ferreira[1]; David Ferras[2]; Dídia I. C. Covas[3]; and Zoran Kapelan[4]

**Abstract:** Stormwater management model (SWMM) software has recently become a modeling tool for the simulation of intermittent water supply systems. However, SWMM is not capable of accurately simulating the air behavior in the pipe-filling phase, missing therefore a relevant factor during pipe pressurization. This work proposes the integration of a conventional accumulator model in the existing SWMM hydraulic model to overcome this gap. SWMM source code was modified to calculate the air piezometric head inside the pipe based on the system boundary conditions, and the air piezometric head was incorporated in the SWMM flow rate pressure component. Experimental data were collected during the rapid filling of a pipe system for three possible configurations that are likely to occur in intermittent water supply pipe systems: no air release, small air release, and large air release. Results show that the improved SWMM better describes the effect of the air behavior using the extended transport (EXTRAN) surcharge method when compared to the original SWMM. Results also show that the SLOT method with predefined slot width is not suitable for this purpose; thus, further research is needed to assess if an adjusted slot width could provide better results. **DOI: 10.1061/JHEND8.HYENG-13137.** 



## Introduction

Pipe-filling events are severe transient events that occur in intermittent water supply, urban drainage, and stormwater systems. The severity comes from high velocities and air pressurization and release that occur during the pipe-filling stage of these systems. As a consequence, mixed flow behavior leads to increased pipe bursts and equipment malfunctioning, especially given that pressure variations can be much higher in the presence of air (Fuertes-Miquel et al. 2019).

Pipe-filling events have been studied in the past based on different modeling approaches: rigid water column (RWC) models, elastic water column (EWC) models, and even more advanced ones, namely, computational fluid dynamics (CFD) models.

The RWC model assumes that the pipe is nondeformable and the liquid is incompressible. This approach was used by Martin (1976) and Cabrera et al. (1992) to analyze the pressurization of a straight water column with an entrapped air pocket described by a simplified accumulator model. The air release with RWC models was firstly quantified by Zhou et al. (2002) using the theory of compressible flows (AGA 1978). Since then, several research works have also been carried out to analyze the effect of trapped and released air during pipe pressurization, concluding that the air behavior is indeed relevant during pipe-filling events (Romero et al. 2020). However, RWC models are not always suitable, particularly in cases in which the wavefront is not always sharp and perpendicular to the pipe axis, as assumed in these models. As noted by Guizani et al. (2006), the wavefront varies with the initial water tank head $H_{ini}$ and the pipe diameter $D$; if the $H_{ini}/D$ ratio is too low, the assumption of a sharp wavefront from the RWC model is not valid, especially in undulating pipe profiles (Liou and Hunt 1996).

The EWC models are able to more accurately simulate unsteady pressure variations in fully pressurized pipes and in pipes with air pocket volumes much smaller than the volume of water. Zhou et al. (2011) analyzed the pressurization and filling of pipes with the elastic model using the method of characteristics to solve the governing mass balance and momentum equations, as it is used for describing water hammer events, though with an additional piston equation to describe the water-air front position. Later, Zhou et al. (2013a) analyzed the pipe-filling events with two separate entrapped air pockets. The effect of blockage and pipe profile was also analyzed by Malekpour and Karney (2014a, b), showing that water column separation can occur and generate subsequent pressure variations that can be significantly higher. However, these researchers still assumed that the wavefront is perpendicular to the pipe axis, which was shown not to be valid for low $H_{ini}/D$ ratios and sloped pipes.

CFD models were also used to simulate pipe-filling events. Martins et al. (2015) developed a conceptual model for pipe pressurization on a pipe dead-end. Martins et al. (2017) further analyzed the same type of system and concluded that the maximum overpressures are a function of the initial air volume, pipe diameter, and level at the upstream tank. Zhou et al. (2018) numerically

[1]Ph.D. Candidate, Dept. of Water Management, Faculty of Civil Engineering and Geosciences, Delft Univ. of Technology, Stevinweg 1, 2628CN Delft, Netherlands (corresponding author). ORCID: https://orcid.org/0000-0002-7889-9218. Email: j.p.ferreira@tudelft.nl

[2]Lecturer, Dept. of Water Supply, Sanitation and Environmental Engineering, IHE Delft Institute for Water Education, Westvest 7, 2611 AX Delft, Netherlands. ORCID: https://orcid.org/0000-0001-9422-3157

[3]Professor, Civil Engineering Research and Innovation for Sustainability, Instituto Superior Técnico, Universidade de Lisboa, Ave. Rovisco Pais 1, Lisbon 1049-001, Portugal. ORCID: https://orcid.org/0000-0001-6901-4767

[4]Professor, Dept. of Water Management, Faculty of Civil Engineering and Geosciences, Delft Univ. of Technology, Stevinweg 1, 2628CN Delft, Netherlands.

Note. This manuscript was submitted on November 17, 2021; approved on September 12, 2022; published online on February 11, 2023. Discussion period open until July 11, 2023; separate discussions must be submitted for individual papers. This paper is part of the ***Journal of Hydraulic Engineering***, © ASCE, ISSN 0733-9429.

analyzed the pipe filling and determined the air-water mixing is not negligible in terms of energy losses in a dead-end pipe system. Indeed, the CFD model's high accuracy makes them useful for descriptive and fundamental research; however, these models are very demanding in terms of time and computational resources, making them unusable for standard engineering practice for water networks.

In contrast, drainage and stormwater systems fillings have been mostly studied using free-surface flow models based on Saint-Venant equations (Ferreri et al. 2010; Vasconcelos and Marwell 2011; Vasconcelos et al. 2018; Pachaly et al. 2019). The frequently used solver for this purpose is EPA's SWMM, which is an open-source software widely accepted by the research and practitioner community. More recently, SWMM has been used to simulate unsteady flow in closed and filled pipes by Pachaly et al. (2021b) and in stormwater systems with an improvement to the slot method by modifying the slot width. Pachaly et al. (2020, 2021a) obtained better results with the SLOT surcharge method, and the importance of Sjöberg's (1982) transition was highlighted for improving numerical stability.

SWMM was proposed as a possible solver to simulate intermittent water supply (IWS) systems by Cabrera-Bejar and Tzatchkov (2009). Campisano et al. (2019) went more in depth and concluded that SWMM is better suited than an RWC model for pipe-filling events since the sharp wavefront assumption is not required in SWMM. More recently, Gullotta et al. (2021) used SWMM to design pressure-reducing valve locations to improve water distribution equity. However, the software still cannot describe the air behavior during pipe-filling events since this kind of interaction has not been yet incorporated in the original SWMM code. Modeling this interaction is relevant in the IWS context since this kind of supply is characterized by three stages: pipe-filling stage, pressurized supply stage, and emptying stage. In practice, only the pressurized supply stage is currently modeled, mostly using EPANET version 2.2, EPA's application for modeling completely continuous pressurized drinking water distribution systems. EPANET model completely disregards the filling and emptying stages, which have a major air-water interaction since air needs to flow in and out of the pipe system.

Overall, previous research widely recognizes the importance of modeling the air behavior in pipe-filling processes; however, to the authors' knowledge, there is no available software (commercial or open source) that integrates the air behavior in free-surface flow models in closed pipes.

The current research aims at the development and validation of experimental data of an improved SWMM model that can simulate the air pressurization process during pipe-filling events. This is achieved by adding the air accumulator model to SWMM's source code. Three configurations of the simple pipe system are analyzed during the pipe-filling process by changing the downstream boundary condition to simulate situations with no air release (dead-end), low air release (small orifice), and high air release (large orifice). These configurations were deemed sufficient to cover different operating configurations that are likely to occur in IWS systems. No consideration was given to more complex systems, such as pipe networks in this work, remaining to be done as part of which will be tackled in future work. The present work represents a proof of concept to assess if SWMM is capable of accurately describing the air behavior during fast pipe-filling events.

The paper is organized as follows. First, the pipe-rig and the experimental data are presented, providing an experimental description of the pipe-filling phenomena and the effect of entrapped air behavior. The original and improved SWMM models are presented. Experimental data and numerical results using the extended transport (EXTRAN) and SLOT surcharge methods are compared, showing the simulation capabilities of the model. Finally, a discussion is held on the importance of improved SWMM for future research, on the key findings, and on the applicability of the proposed model to engineering practice.

## Experimental Data Collection and Analyses

### Experimental Rig

The pipe-rig, depicted in Fig. 1, is composed of an elevated tank, a full bore fast opening DN20 ball valve, pneumatically actuated, a horizontal acrylic pipe with an inner diameter of 21 mm, and a length of 12.4 m.

Pressure measurements were carried out using Siemens SITRANS P pressure transducers Series Z with a maximum measuring range of 0–2.5 m, full-scale accuracy of 0.5%, and time response lower than 0.1 s. Three pressure transducers were installed along the pipe as follows: (1) at the upstream end of the valve to control the tank head (PT1); (2) at pipe midlength (PT2); and (3) at 2.05 m upstream of the pipe end (PT3). Final steady-state flow rate measurements were carried out by a Dynasonic ultrasonic flow meter with a full range accuracy of 1%. All measurements were recorded at a 1 kHz frequency for all tests.

### Collected Data

Two initial water levels in the upstream water tank were tested: $H_{ini} = 0.35$ m and 1.50 m. Five orifice diameters were used as a boundary condition at the downstream end to describe the three possible different air behavior configurations: dead-end, small orifice, and large orifice. These configurations attempt to describe the three possible air release behaviors observed during pipe-filling events (none, small and large air release). Tested boundary conditions at the downstream end, with the respective final steady-state flow rates and Reynolds numbers, Re, are presented in Table 1. These allow to cover flow conditions that go from laminar flow to smooth turbulence. A total of 10 types of experiments were conducted with at least two tests for each configuration type to ensure repeatability. Tests for $H_{ini} = 0.35$ m and for the small orifice configuration show zero flow rate since the flow rate was lower than the flow meter low flow cutoff. Experimental data and corresponding numerical results not shown in the following sections are presented in Figs. S5–S8.

## Pipe-Filling Process and Description

A sample corresponding to the test with tank head $H_{ini} = 0.35$ m was taken to illustrate the dead end and the small and the large air release behaviors.

The observed piezometric heads, $H$, at three measurement locations for the dead-end configuration are presented in Fig. 2. Upon the upstream valve opening (at $t = 0$ s), water flows into the pipe and no air is released. The wavefront advances along the pipe,

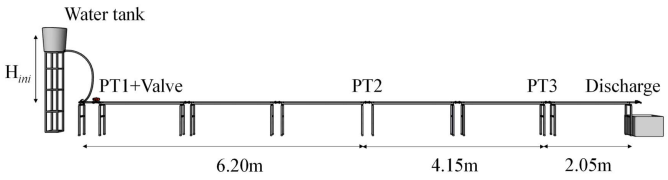


**Fig. 1.** Schematic representation of the pipe-rig layout.

**Table 1.** Experimental tests, steady-state flow rate, and respective Reynolds number

| | Dead end | | Small orifice | | | | Large orifice | | | |
|---|---|---|---|---|---|---|---|---|---|---|
| | d = 0 mm | | d = 1.1 mm | | d = 2.2 mm | | d = 10 mm | | d = 21 mm | |
| $H_{ini}$ (m) | $Q$ | Re | $Q$ | Re | $Q$ | Re | $Q$ | Re | $Q$ | Re |
| 0.35 | 0 | 0 | 0 | 0 | 0 | 0 | 0.28 | 4,715 | 0.37 | 6,231 |
| 1.50 | 0 | 0 | 0.03 | 488 | 0.08 | 1364 | 1.02 | 17,178 | 1.23 | 20,715 |

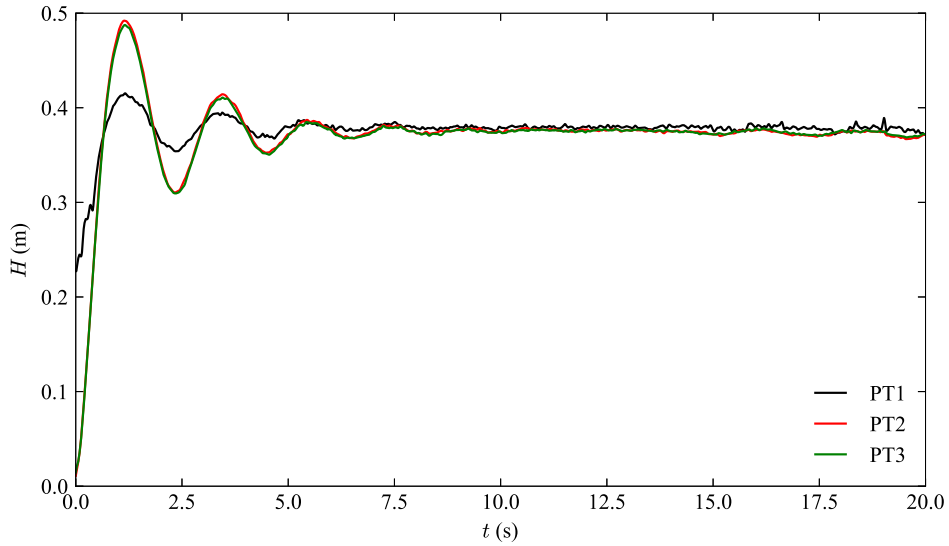


**Fig. 2.** Experimental piezometric head in dead-end configuration.

and the air immediately starts to compress. While compressing, the air behaves as an energy accumulator, and once the kinetic energy of the water column from the valve opening has been transferred into potential energy in the air phase (at $t = 1.3$ s), the wavefront starts to move backward as the air starts to expand. This cycle repeats itself until the kinetic energy is dissipated through friction and a final steady state is reached with a balanced air pocket pressure and water level at the tank. Hardly any difference between PT2 and PT3 measurements can be seen in Fig. 2 since the wavefront does not reach any of the transducers and both measure the air piezometric head as a single fluid. This quasi-steady assumption is valid since the air celerity becomes $\sqrt{K_{air}^{adiabatic}/\rho_{\text{air}}} = \sqrt{142000/1.42} = 314$ ms$^{-1}$ for adiabatic processes and becomes $\sqrt{K_{air}^{isothermal}/\rho_{air}} = \sqrt{101000/1.42} = 267$ ms$^{-1}$ for isothermal processes. Thus, air pressure longitudinal variation takes a maximum of 12.4 m/267 ms$^{-1}$ = 0.046 s from the start of the air-water interface to the air pocket downstream end. Such time is of an order of magnitude around 100 times lower than the water wavefront advance in the pipe, making the spatial variation of the air pressure negligible in the current tests. Thus, whenever the air piezometric head is compared to the dead-end configuration, only data from one transducer will be presented.

A sample of data collected for the pipe-filling event with a small air release configuration is shown in Fig. 3. The registered piezometric head corresponds to the fluid piezometric head: first the air's and then the water's, when it reaches each transducer location. Once the valve opens (at $t = 0$ s), the wavefront starts advancing along the pipe and the air pressure increases. The small orifice at the downstream end allows the air release even though the air piezometric head inside the pipe reaches values similar to the ones of the water in the tank. When the air pressure inside the pipe and the tank level reach an equilibrium (approximately at $t = 2$ s), the flow rate severely decreases due to the smaller pressure gradient. While the wavefront progresses, the air piezometric head decreases until the wavefront arrives at each measuring location due to the air release at the downstream end. When the water arrives at each transducer, the registered pressure remains relatively constant. Air pressure decreases at a much faster pace due to its release, while the water pressure corresponds to the water tank level subtracted from head losses until the transducer. Thus, the wavefront arrives at PT2 at $t = 10$ s and at PT3 at $t = 34$ s. When the wavefront reaches the downstream end at $t = 39$ s, a severe pressure surge is observed due to a small volume of air trapped at the downstream end that rapidly compresses and cannot be released as the orifice creates the same effect as a blockage, creating the observed pressure spikes between $t = 39$–55 s. Through visual observation during each test, some air volume remains in the pipe in the form of small bubbles scattered at the upper side of the pipe.

Different behavior is observed in Fig. 4 that shows a sample of the collected data for the larger orifice configuration. After opening the valve, the pipe starts to rapidly fill, and no pressurization is observed until the water wavefront arrives at PT2 and PT3 at $t = 5$ s and $t = 14$ s, respectively. Then, the pressure head slowly increases at PT2 and PT3 until the wavefront reaches the pipe end ($t = 18$ s). Once the pipe end is reached, the pressure oscillates sharply due to a sudden variation in the local head loss created by the orifice. The gradual pressure head reduction after $t = 18$ s represents the upstream water tank emptying.

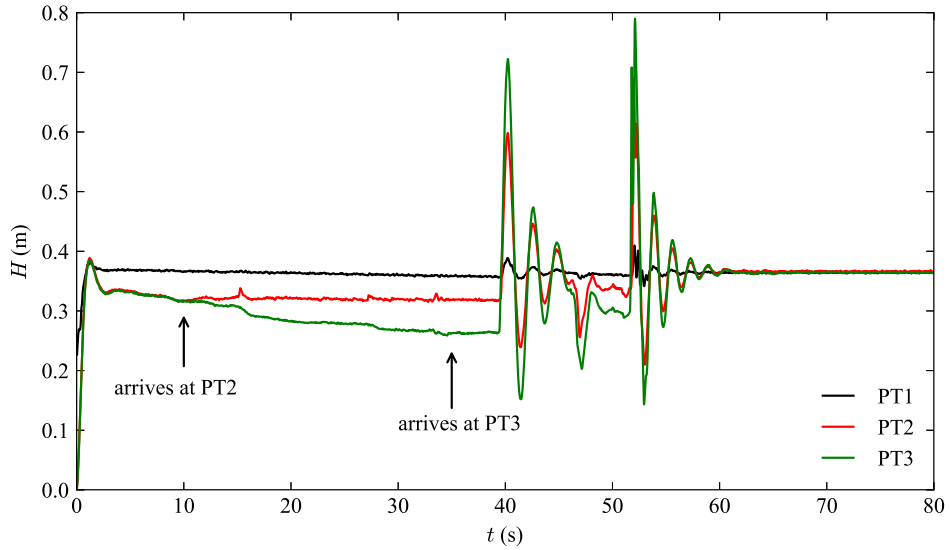


**Fig. 3.** Experimental piezometric head in small orifice configuration.

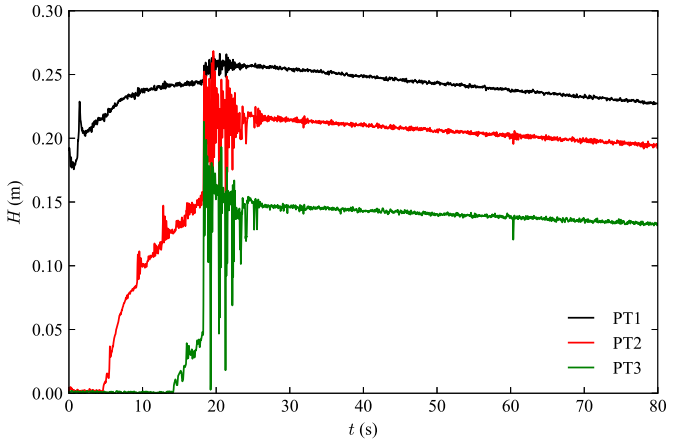


**Fig. 4.** Experimental piezometric head for large orifice configuration.

## Air Modeling Methodology

### *Air Behavior Model*

The simplified accumulator model with compressible flow theory for air release through orifices is used herein to simulate the air behavior during the pipe-filling process. In this approach, only the polytropic coefficient (which is considered constant) is required.

Water flow is considered incompressible in the Saint-Venant equations. Since the air is several times more compressible than water, the variation of the air volume inside the pipe can be described by the piston function

$$\frac{d\forall_a}{dt} = -Q_w \tag{1}$$

in which $\forall_a$ = air volume inside the pipe; $t$ = time; and $Q_w$ = water flow rate.

Air release formulation depends on the downstream orifice size and the air pressure inside the pipe, $p_a$. Considering atmospheric pressure, $p_{atm}$, when $p_a/p_{atm} < 1.89$, the air release from an orifice occurs in subsonic conditions, and the air behavior can be described as an isentropic behavior (Binder 1955). Under these conditions, airflow is described as follows (Zhou et al. 2002):

$$Q_a = C_d A_0 Y \sqrt{2g \frac{\rho_w}{\rho_a} \frac{(p_a - p_{atm})}{\gamma_w}} \tag{2}$$

$$Y = \left[ \frac{k}{k-1} \left( \frac{p_{atm}}{p_a} \right)^{2/k} \frac{1 - (p_{atm}/p_a)^{(k-1)/k}}{1 - (p_{atm}/p_a)} \right]^{1/2} \tag{3}$$

where $Y$ = expansion factor (Martin 1976); $Q_a$ = air flow rate released from the orifice; $C_d$ = discharge coefficient; $A_0$ = cross section area of the orifice; $g$ = gravitational acceleration; $\rho_a$ = air density; $\rho_w$ = water density; and $k$ = polytropic coefficient.

In the other case, when $p_a/p_{atm} \geq 1.89$, the flow through the orifice becomes chocked and a maximum air flow rate can be released

$$Q_a = C_d A_0 \sqrt{g \frac{\rho_w}{\rho_a} p_a} \sqrt{k \left( \frac{2}{k+1} \right)^{(k+1)/(k-1)}} \tag{4}$$

According to Eq. (1), the air volume varies as a function of the water flow rate, which, in turn, becomes a function of the air flow and the air compression, due to the two-way interaction between the water and air. Therefore, the air pressure $p_a$ and the air density $\rho_a$ vary with time as follows:

$$\frac{dp_a}{dt} = \frac{p_a k}{\forall_a} (Q_w - Q_a) \tag{5}$$

$$\frac{d\rho_a}{dt} = \frac{\rho_a}{\forall_a} (Q_w - Q_a) \tag{6}$$

The used polytropic coefficient $k$ is considered constant for each test. Since most transient water dynamics have an initial faster behavior immediately after a changing boundary condition maneuver, for which the flow is adiabatic, and a slower one during the establishment of the final steady state, behaving as an isothermal process, most authors propose a $k = 1.2$ for unsteady flow events in pipes (Chaudhry 2014). Nonetheless, the polytropic coefficient

value will be calibrated in this work for the three analyzed pipe configurations.

## Existing SWMM Model

### Basic Equations and Recommendations

The existing SWMM model is based on the following Saint-Venant equations corresponding to the mass and momentum continuity equations of free-surface flows

$$\frac{\partial A}{\partial t} + \frac{\partial Q_w}{\partial x} = 0 \tag{7}$$

$$\frac{\partial Q_w}{\partial t} + \frac{\partial (Q_w^2/A)}{\partial x} + gA\frac{\partial H}{\partial x} + gAS_f = 0 \tag{8}$$

where $A$ = flow cross section area; $t$ = time; $x$ = length; $H$ = piezometric head; and $S_f$ = friction slope.

In the numerical scheme, the water flow rate is calculated by an implicit backward Euler numerical scheme (Roesner et al. 1988; Rossman 2017). The solver calculates the flow rate for all the pipe segments in the system (herein referred to by pipe $p$) in the order in which the pipes were introduced in the input file, for each time step, $t+1$, and based on the previous time step, $t$

$$Q_{t+1,p} = \frac{Q_{t,p} + \Delta Q_{t,p}^{inertia} + \Delta Q_{t,p}^{pressure}}{1 + \Delta Q_{t,p}^{friction}} \tag{9}$$

in which $\Delta Q_{t,p}^{inertia}$ = inertial component of the flow rate which varies with the mean flow velocity in pipe $p$ and with the flow area and flow rate changes between time steps; $\Delta Q_{t,p}^{pressure}$ = flow rate component of the calculation in which the differential pressure between upstream and downstream nodes of pipe $p$; $\Delta Q_{t,p}^{friction}$ = head loss component of the flow rate calculation where only the wet perimeter (without the air) should be considered, even if the air inside the pipe $p$ is pressurized; and $p$ = pipe in the node sequence in analysis.

A surcharge method is required when the pipe is pressurized. SWMM version v5.1.015 includes two surcharge methods: EXTRAN and SLOT. The EXTRAN surcharge method uses the continuity and the momentum equations to calculate the piezometric head, assuming a full pipe cross section, making the convective terms of the equations equal to zero. Roesner et al. (1988) recommended a maximum time step $\Delta t = L/\sqrt{gD}$ to ensure numerical stability when using this method, in which $L$ is the pipe length and $D$ is the pipe's inner diameter. Vasconcelos et al. (2018) found the previous recommendation to be inaccurate for rapid pipe filling and recommended a time step reduced tenfold

$$\Delta t = 0.1\frac{L}{\sqrt{gD}} \tag{10}$$

Conversely, the SLOT surcharge method uses the Preissmann slot method to solve pressurized pipe flow while using Saint-Venant equations. An artificial slot is assumed on top of each pipe $p$ to represent the pressurized pipe flow as free-surface flow. As such, the model still uses the convective term of Saint-Venant equations, but the flow area now incorporates the slot width $T_s$. The value proposed by Sjöberg (1982) is used herein, as predefined in SWMM. More information on SWMM and the respective surcharge methods can be found in Rossman (2017).

Both surcharge methods should provide similar results for steady pressurized pipe flows, being the SLOT method preferential. However, such slot width does not allow us to accurately estimate piezometric heads in fast unsteady pipe flows. For such dynamic events, the recommended slot width has been recommended should the following (Aureli et al. 2015):

$$T_s = \frac{gA}{c_p^2} \tag{11}$$

where $c_p$ = pipe wave celerity.

Since the wave celerity has been changed from the celerity of free-surface flows to the pipe pressure wave celerity and consequently the slot width, the minimum time step must be adjusted. Reducing the slot width requires smaller time steps to comply with Courant's number lower or equal to the unit $Cr = c_p/(\Delta x/\Delta t) \le 1$. Thus, pipe segments of $\Delta x = 0.2$ m require a minimum time step of $\Delta t = 0.00066$ s for the pipe pressure wave celerity. Instabilities were observed for this time step, but no reference could be found on this concern. Thus, a sensitivity analysis using the original SWMM with different time steps was carried out to demonstrate that this is a limitation of the original SWMM and not of the improved version.

### Time Step Sensitivity Analysis

A sensitivity analysis of the time step was carried out to assess its influence on the pipe-filling process. Fig. S1 shows the piezometric head at PT2 and PT3 for time steps, $\Delta t$, ranging from 0.0005 to 0.045 s. Results for $\Delta t = 0.0005$ s (very close to the required time step of $\Delta t = 0.00066$ s by the adjusted SLOT method) are not numerically stable. Only time steps higher than 0.01 s show no significant numerical instabilities for the space step of $\Delta x = 0.2$ m. The time step $\Delta t = 0.00066$ s is significantly below the simulation conditions for which SWMM is numerically stable for the spatial discretization considered in this paper's simulations.

### Spatial Discretization Sensitivity Analysis

A sensitivity analysis of the spatial discretization was also carried out to assess its influence on the pipe-filling process, and the results are shown in Fig. S2. The three configurations (dead end, small orifice, and large orifice) were tested using both EXTRAN and SLOT surcharge methods. Spatial steps, $\Delta x$, were varied from 0.01 m to 0.4 m, corresponding to $\Delta x/D$ between 0.47 and 19.05. The formula for obtaining the spatial discretization that leads to the most accurate results was recommended by Vasconcelos et al. (2018), resulting in $\Delta x = 0.2$ m for the specific setup of this study. Note that other systems/studies are likely to require a different spatial discretization $\Delta x$. EXTRAN surcharge method consistently provided better and more stable results than the SLOT method, for which excessive head losses were observed for the dead-end configuration, and numerical instabilities were obtained for the small orifice configuration for the discretization with smaller space steps ($\Delta x/D$<9.52). No instabilities or excessive head losses were observed for finer spatial discretizations with the EXTRAN surcharge method even though results were not as accurate as for $\Delta x/D$<9.52. All simulations for the spatial discretization analysis required an adjustment of the time step according to Eq. (10).

## Improved SWMM Model—AirSWMM

To incorporate the air behavior in the SWMM model, the pressure component of the flow rate calculation $\Delta Q_{t,p}^{pressure}$ from Eq. (9) needs to be modified

$$\Delta Q_{t+1,p}^{pressure} = -gA\frac{H_{2;t,p} - H_{1;t,p}}{L}\Delta t \tag{12}$$

where $H_{1;t,p}$ and $H_{2;t,p}$ = piezometric heads at the upstream and downstream end of the pipe $p$, respectively, at the previous time step.

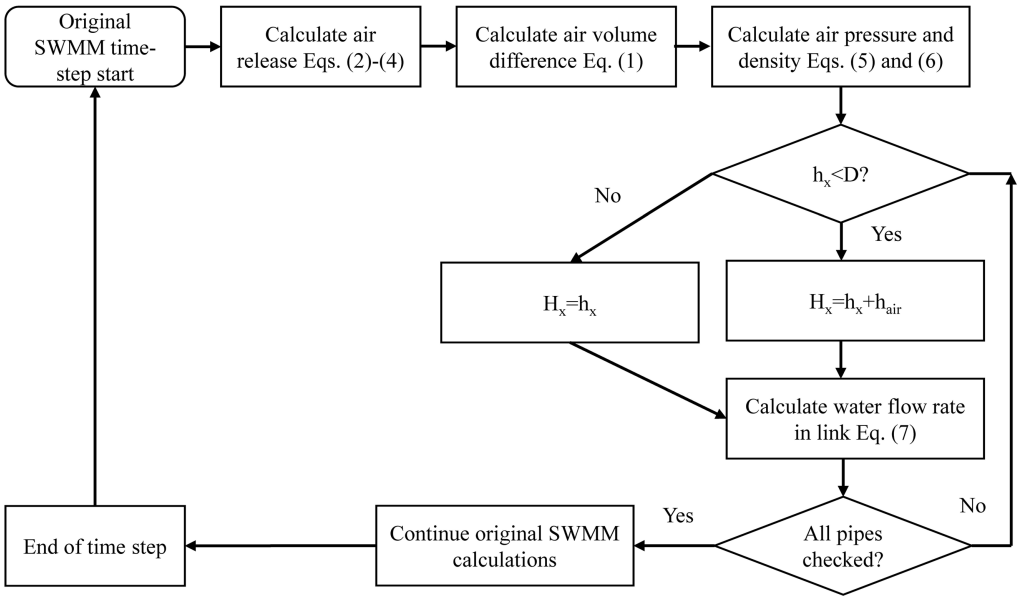


**Fig. 5.** Implementation chart for the air phase calculation in AirSWMM.

The incorporation of air pressure in the model requires the consideration of three different cases: (1) Case I, where both nodes of the pipe are filled with water (i.e., pressurized water column), (2) Case II, when only one side of the pipe is full of water, and (3) Case III, when both nodes have free-surface flow. Case I does not require the correction of the air pressure term since the pipe is already pressurized and no trapped air is considered. In Cases II and III, the air pressure head should be added to the piezometric head in the nodes in contact with air for the flow rate calculation. Thus, the piezometric heads from Eq. (12) need to be corrected to $H = h_x + h_{\text{air}}$, where $h_x$ corresponds to the water depth at the calculation node obtained from SWMM and $h_{air} = (p_a - p_{atm})/(\rho_a g)$ corresponds to the air pressure inside the pipe. The calculation process for the improved SWMM model is depicted in Fig. 5. AirSWMM will be used as the model's name for SWMM with the air behavior implementation.

## Results

Three different configurations (dead-end, small orifice, and large orifice) with tank head $H_{ini} = 0.35$ m were simulated using both the original SWMM and the AirSWMM model with $H_{ini} = 0.35$ m. The obtained numerical results are compared with the corresponding collected data.

The experimental pipe-rig could be modeled using a single straight horizontal pipe between two nodes. However, the pipe was discretized in 62 pipe segments with lengths of $L = \Delta x = 0.2$ m between 63 nodes to improve the solver accuracy with dummy nodes between each stretch of the pipe as proposed by Pachaly et al. (2020). The used time step for the small and large orifice configurations is calculated using Eq. (10), resulting in a maximum time step of $\Delta t = 0.044$ s.

The water tank, upstream boundary condition, was modeled by its initial water level obtained from PT1 and by the tank geometry. Both original and AirSWMM models use a local head loss coefficient, $K$. Parameter $K_{\text{up}}$ was introduced in the first pipe segment to represent the local head losses from the tank to the pneumatically actuated valve, and parameter $K_{down}$ was introduced in the last pipe segment to describe the orifice head loss. The wave celerity when the pipe is pressurized was considered as $c_p = 300$ ms$^{-1}$, calculated by a theoretical formula based on the water properties and the pipe characteristics, and was attributed to all pipe segments.

The polytropic coefficient $k$ was observed not to vary significantly from the $k = 1.2$ recommended in the literature (Chaudhry 2014). However, when no air release exists, the polytropic coefficient that best describes the observed behavior is 1.0. This is explained by the fact that, during the pipe filling, the adiabatic assumption for the air behavior is no longer valid, as there is heat transfer from the water to the air and to the pipe walls (Zhou et al. 2013b). A sensitivity analysis of the $k$ parameter is presented in the Supplemental Materials for the dead-end and small orifice configuration (Figs. S3 and S4). Results for the pipe system with the large orifice configuration are not presented because these are insensitive to $k$ values since no relevant pressure variations in the air column are observed in these tests.

### Calibration and Validation

To determine the performance of the proposed changes in AirSWMM, the tests for $H_{\text{ini}} = 0.35$ m of the collected data were used to calibrate the model and the second half ($H_{ini} = 1.5$ m) for its validation. Given the limited number of sensors in the system, no optimization was run. The calibration was carried out by using a trial-and-error approach assessing the calibration by means of minimizing the root mean square error (RMSE). The validation process was carried out by using the parameters determined during the calibration process. The predetermined parameters are the time step, the spatial discretization, according to Eq. (10), and the absolute roughness of the pipe, estimated by the steady state at the end of each test. The calibration parameters are the local head loss coefficients and the polytropic coefficient.

The time step, spatial discretization, absolute roughness of the pipe, local head loss coefficients, and polytropic coefficients used in the numerical simulations are presented in Table 2. As an exception, a time step of $\Delta t = 0.001$ s is required for the dead-end configuration since the waterfront does not advance enough in the calculation nodes. This can also be confirmed with the ideal gas law $(p_f - p_i)(V_f - V_i) = kRT$ in which $p$ is the air pressure inside the pipe, $V$ is the air volume, $R$ is the ideal gas constant, and $T$ is the

**Table 2.** Estimated calibrated SWMM model parameter values

| Model parameter | Parameter | Test | | | | |
|---|---|---|---|---|---|---|
| | | d = 0 mm | d = 1.1 mm | d = 2.2 mm | d = 10 mm | d = 21 mm |
| $\Delta t$ (s) | Eq. (10) | 0.001 | 0.044 | 0.044 | 0.044 | 0.044 |
| $\Delta x$ (m) | Model input | | | 0.2 | | |
| Absolute roughness (m) | Estimated | | | 0.00076 | | |
| $K_{up}$ | Calibrated | | | 4 | | |
| $K_{down}$ | Calibrated | 10,000 | 200 | 200 | 13 | 0 |
| $k$ | Calibrated (AirSWMM) | 1.01 | 1.15 | 1.15 | 1.2 | 1.2 |

temperature. The waterfront advances only 0.25 m, which is hardly more than a single space step (0.2 m).

### Dead-End Configuration Results

Experimental data and numerical results for original SWMM and AirSWMM in the case of dead-end configuration (i.e., no air escape) are presented in Fig. 6.

Numerical results obtained by the EXTRAN surcharge method for the dead-end configuration are depicted in Fig. 6(a). The original SWMM is not capable of simulating the observed air-water behavior since it assumes an atmospheric piezometric head ahead of the water column during the pipe filling. The calculated piezometric head is zero until the water column reaches the location of PT3 at $t = 16.0$ s. When the wavefront reaches the downstream end of the pipe ($t = 19.0$ s), a transient pressure wave, corresponding to the filling wave going against the dead end, occurs. However, this transient phenomenon is not well described by the original SWMM model because the previous stage is not properly reproduced. Conversely, AirSWMM results show a good agreement between the calculated air piezometric head and the experimental data for the first two wave periods: there is no energy loss during the pipe filling, and the air pocket behaves simply as an energy accumulator. After the first two wave periods, the AirSWMM numerical model shows some discrepancies in amplitude and phase with the observed pressure head mostly due to the underestimation of the energy dissipation since the air behaves as a simple energy accumulator and not as a dissipator.

Numerical results obtained by the SLOT surcharge method for the dead-end configuration are presented in Fig. 6(b). The original SWMM model is not capable of simulating the observed behavior once again. Even though AirSWMM results with the predefined Preissmann slot show a better agreement with the collected data, obtained accuracy is not satisfactory enough as neither the pressure wave amplitude nor the period agrees well with the experimental pressure wave behavior. Results do not improve when adjusting the slot width to the one proposed by Aureli et al. (2015). This is

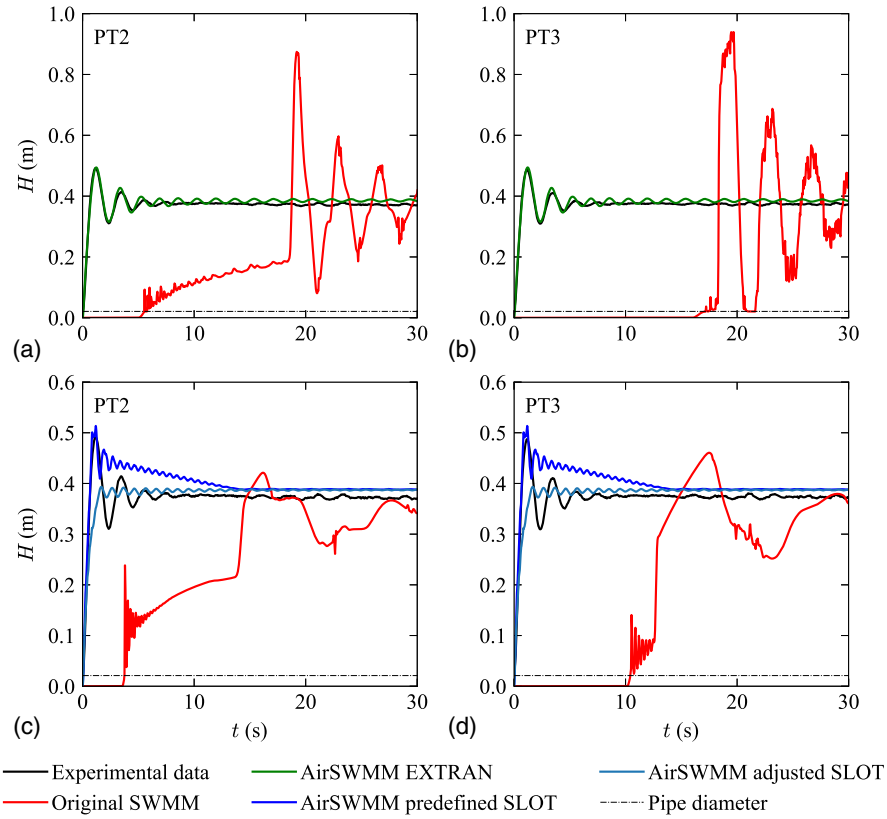


**Fig. 6.** Experimental data versus numerical results for $H_{ini} = 0.35$ m and dead-end configuration: (a and b) with the EXTRAN model at PT2 and PT3; and (c and d) with SLOT method with SWMM predefined slot width and with the adjusted slot width at PT2 and PT3.



J. Hydraul. Eng., 2023, 149(4): 04023004

because, in order to use the adjusted slot, the time step needs to be significantly reduced ($\Delta t = 0.00066$ s $= \Delta x/c_p$) to comply with the Courant condition. Such a small time step leads to numerical dispersion in SWMM, which has also been observed by other researchers in SWMM community discussions. Using longer and larger diameter systems will allow understanding if the adjusted slot is adequate in a broader context. Overall, the SLOT method is not capable of describing the filling event for the dead-end configuration.

### Small Orifice Configuration Results

The comparison between the original SWMM and AirSWMM results with collected experimental data for the small orifice configuration (i.e., limited air release) is shown in Fig. 7.

Results for the EXTRAN surcharge method used in two SWMM models are shown in Fig. 7(a). As can be seen from this figure, the original SWMM model cannot reproduce the air behavior since it assumes the air is at the atmospheric pressure inside the pipe during the filling phase. Also, the arrival time of the wavefront does not agree with the collected data: the wavefront reaches PT3 at $t = 12.5$ s in the original SWMM model, while the experimental data shows the wavefront arrives at that location at $t = 34$ s. When the wavefront reaches the downstream end, a transient is generated but does not have the same impact as in the dead-end configuration because there is still flow going through the orifice. Conversely, AirSWMM (with EXTRAN surcharge method) can describe the observed behavior reasonably well, given the good agreement with experimental data for the first overpressure caused by the air compression ($t = 1$ s). Once the wavefront reaches each transducer, the piezometric head stops decreasing becoming constant since the measured piezometric head no longer corresponds to the one from the air but from the water, belonging directly to the one from the water tank. After the pipe pressurization (at $t = 39$ s), a pressure surge is observed in both pressure transducers. This corresponds, once again, to the wavefront reaching the orifice. However, in this situation, the pressure variation is only roughly approximated by the experimental results. After the pressure surge at $t = 39$ s, the observed pressure variations are a consequence of some small air pockets being released. While the air is released, the water flow rate is affected by an air bubble generating a pressure surge that is immediately alleviated by the air release and the restitution of the flow. The wavefront arrival time is also accurately predicted using the AirSWMM model.

Results obtained using the SLOT surcharge method for the small orifice configuration are shown in Fig. 7(b). Neither the original SWMM nor AirSWMM can describe well the pipe-filling process for this configuration. The wavefront predicted by the original SWMM arrives at PT3 around $t = 23$ s, whereas the actual wavefront arrives at $t = 34$ s. Also, the correct steady-state piezometric head is never reached. Despite some numerical instabilities, AirSWMM describes reasonably well the initial stage of air pressurization (until $t = 15$ s). Observed numerical instabilities are likely to be a consequence of the flow rate variation and the piezometric head calculation with the SLOT method. These instabilities are not improved even if several calculation iterations are made for each time step. Therefore, the SLOT method is not capable of describing the pipe-filling event for the small air release configuration.

### Large Orifice Configuration Results

Fig. 8 shows the comparison between the experimental data and the numerical results from the original SWMM and AirSWMM for the large orifice configuration. Fig. 8(a) shows the results in the case of the EXTRAN surcharge method, whereas Fig. 8(b) shows the corresponding result when the SLOT surcharge method is used.

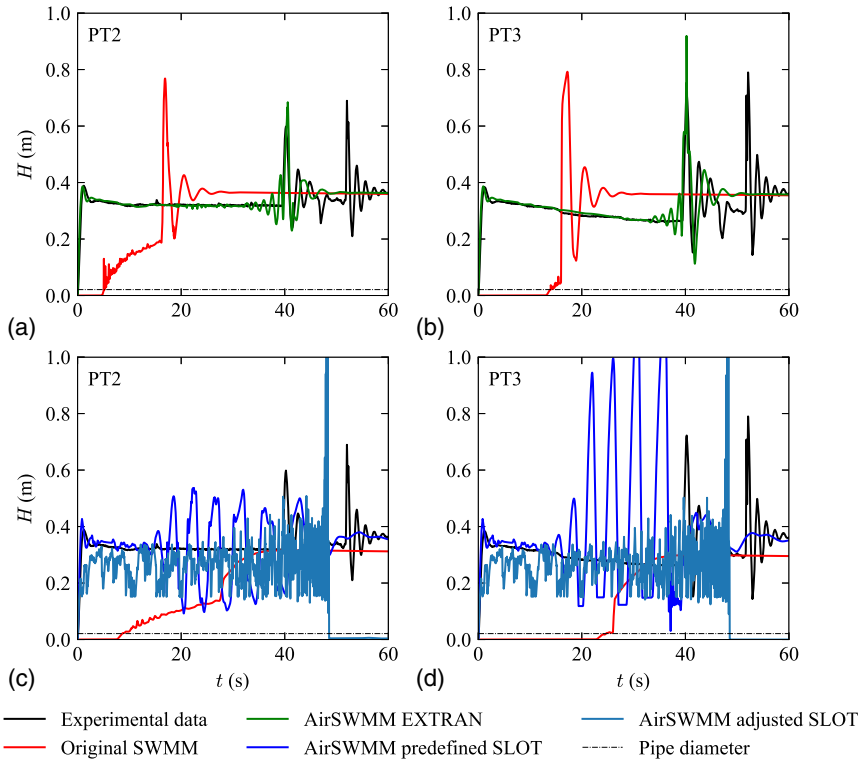


**Fig. 7.** Experimental data versus numerical results for $H_{ini} = 0.35$ m and small orifice configuration: (a and b) with EXTRAN model at PT2 and PT3; and (c and d) with SLOT method with SWMM predefined slot width and with the adjusted slot width at PT2 and PT3.



J. Hydraul. Eng., 2023, 149(4): 04023004

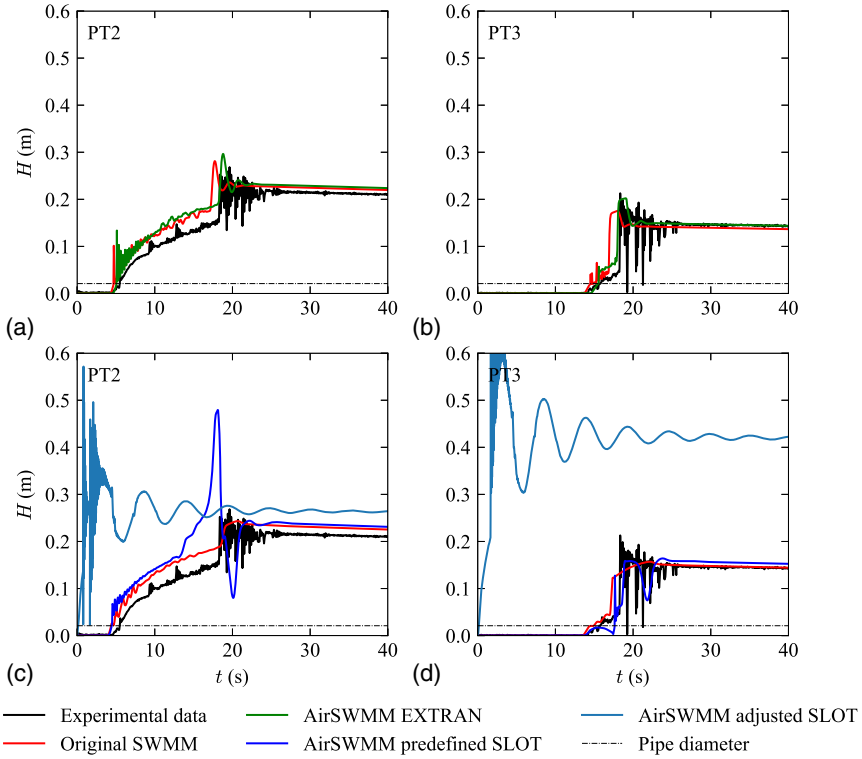


**Fig. 8.** Experimental data versus numerical results for $H_{ini} = 0.35$ m and large orifice configuration: (a and b) with the EXTRAN model at PT2 and PT3; and (c and d) with SLOT method with SWMM predefined slot width and with the adjusted slot width at PT2 and PT3.

Both original SWMM and AirSWMM with EXTRAN surcharge methods can describe the pipe-filling behavior in terms of pressure heads. The piezometric head slightly increases after the valve opening ($t = 0$ s) because the water inflow and the air release predictions are decoupled. The calculated wavefront arrives at the pressure transducers at the same time as observed in the experimental data.

On the one hand, results from the original SWMM, using the SLOT surcharge method, are numerically stable and agree, to a certain extent, with the experimental data. The arrival time is correctly estimated, but the arrival at the downstream end is anticipated. On the other hand, results from AirSWMM are not numerically stable, and hence, this model is not capable of simulating well the pipe-filling process. Therefore, once again, the SLOT method is not suitable for describing the filling event when used with the AirSWMM model.

### *AirSWMM Validation*

Previous sections have demonstrated the predictive performance of AirSWMM for the dataset used for calibration. This section assesses the performance of this model with the validation dataset (i.e., not used in the calibration process), including collecting data for the initial water tank level of $H_{ini} = 1.50$ m. Fig. 9 shows the comparison of predictions obtained using the AirSWMM model with the EXTRAN surcharge method with the corresponding experimental data, all for the three analyzed configurations.

Figs. 9(a and b) shows the numerical results with experimental data for the dead-end configuration. AirSWMM is still capable of describing well the air behavior during the pipe pressurization. The piezometric head amplitude is still correctly estimated, but the wave period is slightly delayed. A different polytropic coefficient value is needed to address this, as a faster pipe-filling event makes the thermodynamic process more adiabatic. As a result, the polytropic coefficient $k$ of 1.0 is found more appropriate for this specific case. Even though the polytropic coefficient may vary, the overall behavior is not deeply affected as observed in Figs. S3 and S4. Hence, a value of $k = 1.2$ is recommended.

The numerical results and experimental data for the small orifice configuration are shown in Figs. 9(c and d). Again, AirSWMM is able to describe the air behavior during pipe pressurization. In the AirSWMM results, the pressure amplitude is correctly estimated after the valve opening. However, the pipe fully pressurizes sooner than observed in the experimental data. Such a time difference is due to the calibrated polytropic coefficient, $k$, for $H_{ini} = 0.35$ m: the value of this coefficient not only influences the air pressurization and the air density but also affects the air release estimated by Eq. (12). Hence, the $k$ value influences the pipe filling in two different ways. Still, the observed piezometric heads and the time of arrival have clear improvements using the AirSWMM model when compared to the original SWMM results.

Figs. 9(e and f) compares the numerical results and experimental data for the large orifice configuration. AirSWMM still has some air pressurization during pipe filling, but both the arrival time and the pressurization time agree with experimental data. The model estimated the correct steady-state piezometric head, but does not reproduce the pressure peak when the wavefront reaches the downstream end.

The RMSE between experimental and numerical data for the simulations with the EXTRAN surcharge method are included in Table 3. Calibration parameter values show the worst agreement for the small orifice configuration in general, but that is due to the hydraulic transient generated when the waterfront wave reaches the orifice. Nevertheless, validation numerical results still present a good agreement with experimental data.

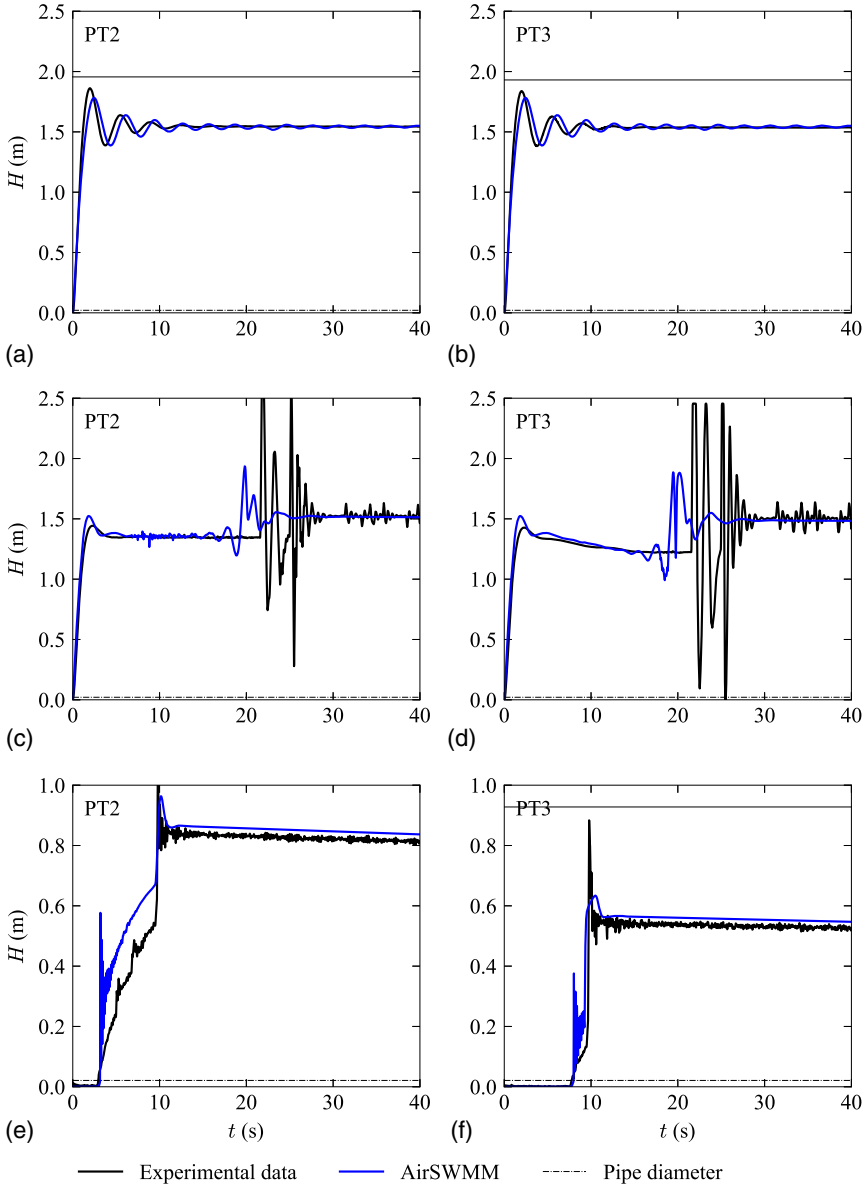


**Fig. 9.** Experimental data versus numerical results for $H_{ini} = 1.50$ m: (a and b) with the EXTRAN model at PT2 and PT3 for dead-end configuration (d = 0 mm); (c and d) with the EXTRAN model at PT2 and PT3 for small orifice configuration (d = 1.1 mm); and (e and f) with the EXTRAN model at PT2 and PT3 for large orifice configuration (d = 10 mm).

**Table 3.** RMSE values from calibration and validation comparison between collected experimental data and numerical results

| $H_{ini}$ | Dead end | Small orifice | | Large orifice | |
|---|---|---|---|---|---|
| (m) | d = 0 mm | d = 1.1 mm | d = 2.2 mm | d = 10 mm | d = 21 mm |
| 0.35 | $1.8 \times 10^{-4}$ | $2.0 \times 10^{-3}$ | $1.5 \times 10^{-2}$ | $2.7 \times 10^{-4}$ | $4.9 \times 10^{-4}$ |
| 1.50 | $1.6 \times 10^{-3}$ | $2.8 \times 10^{-2}$ | $6.0 \times 10^{-2}$ | $2.0 \times 10^{-3}$ | $2.9 \times 10^{-4}$ |

## Discussion

SWMM has been used as a solver for the modeling of IWS systems, especially for the description of the pipe-filling stage (Cabrera-Bejar and Tzatchkov 2009; Campisano et al. 2019). Previous contributions using SWMM assume air is released at each calculation node, which is not always the case in IWS systems, leading to inaccurate results. Even though the present work addresses only water filling in a single pipe (or several pipes in series), this methodology could be extended to pipe networks by creating multiple air pockets, tracking the flow path into multiple branches, and adjusting the flow rate accordingly.

The incorporation of the air behavior in SWMM will allow a better simulation of pipe-filling events for three reasons. First, air in pipes is one of the main causes of pipe operation disruptions and pipe failures (Fuertes-Miquel et al. 2019), which were shown to increase from 30% to 70% for water mains and household connections in IWS operation (Christodoulou and Agathokleous 2012). Incorporating the air behavior will allow us to better estimate the air pressure in the pipes and the definition of measures to prevent unusually high pressures that lead to pipe failures. Second, entrapped air pockets also create additional head losses in the system that only aggravate the already low pressures in IWS systems since head losses can be 20%–35% higher than in air-free pipes (Stephenson 1997; Pothof and Clemens 2010). Such losses could

be obtained by estimating the air volume in the pipes using AirSWMM. This estimation allows for better quantification of pressures at each service connection and, hence, a better determination of the supplied water volume. Finally, IWS creates great social equity problems between service connections closer to storage tanks and those at the network outskirts (Sharma and Vairavamoorthy 2009). AirSWMM allows a more accurate estimation of the system filling time due to the air release, thus providing better means to define measures to improve IWS equity.

Thus, AirSWMM is an improved modeling tool for IWS system designers, consultants, and utilities. This applies to both: (1) the redesign of existing WDS that were designed originally for continuous water supply but had to be converted into IWS for various reasons (Andey and Kelkar 2007); and (2) the design of new IWS systems when other constraints like water shortage, power instabilities, and unreliable water treatment reagents supply chain (Simukonda et al. 2018).

Based on the presented experimental and numerical analyses, the authors advocate the use of AirSWMM, including compressible flow theory for the air behavior description and the EXTRAN surcharge method for the description of pressurization transitions, as a most convenient trade-off between theory and practice when undertaking numerically pipe-filling analyses and air volume quantification.

## Conclusions

Air behavior is of great relevance in pipe-filling events, and simulations are required to estimate maximum and minimum pressure variations generated by the presence of air. So far, there are no available modeling tools to simulate the pipe-filling operations of IWS systems considering the air-water behavior. The present research experimentally describes the effect of air during the pipe-filling process, confirming its relevance based on three scenarios: no air release, small air releases, and large air releases. An explanation of the phenomenon is provided by the development of an improved SWMM code that includes compressible flow theory for air release. After experimental verification, the model has proven to have good predictive potential in estimating pressure variations and the time arrival of the filling and pressurization of the system. Based on the results obtained, the following conclusions are drawn:

1. AirSWMM model with the EXTRAN surcharge method can reproduce well the observed experimental data for the three analyzed pipe-filling cases. This applies to predicting piezometric heads, wavefront arrival times, and pressurization time.
2. When compared to the original SWMM model, the AirSWMM model shows a significant performance improvement in terms of all aforementioned predictions, which is important for modeling pipe filling in real IWS systems, as elaborated in the discussion section.
3. AirSWMM model with the SLOT surcharge method cannot accurately describe the pipe-filling event in any of the analyzed configurations. When compared to experimental data, either the numerical piezometric heads were overestimated or the solver had numerical instabilities that turned it virtually unusable.

Further research is required to assess if an adjusted Preissmann slot width could be valid by using higher time steps for larger systems (i.e., higher than the minimum required to ensure numerical stability). More importantly, the AirSWMM model shown needs to be further developed to simulate the pressure and flow rate conditions in the presence of air in more complex IWS systems, like pipe networks, and also for pipe emptying events, as air entrainment might also play an important role during such processes.

## Data Availability Statement

All experimental data and numerical results, models, and code that support the findings of this study are available from the corresponding author upon reasonable request.

## Acknowledgments

The authors acknowledge the Portuguese national funding agency, Fundação da Ciência e Tecnologia (FCT), for funding the reported work within Grant No. SFRH/BD/146709/2019.

## Notation

*The following symbols are used in this paper:*

$A$ = pipe cross section area ($m^2$);
$A_0$ = cross section area of the orifice ($m^2$);
$C_d$ = orifice discharge coefficient;
$c_p$ = pipe wave celerity ($m\,s^{-1}$);
$c_w$ = shallow water wave celerity ($m\,s^{-1}$);
$D$ = pipe diameter (m);
$g$ = gravitational acceleration ($m\,s^{-2}$);
$H$ = piezometric head (m);
$H_{ini}$ = initial water tank head (m);
$h_{air}$ = air piezometric head (m);
$k$ = polytropic coefficient;
$K_{up}, K_{down}$ = local head loss coefficients;
$L$ = pipe length (m);
$p_a$ = air pressure (Pa);
$p_a$ = atmospheric pressure (Pa);
$Q$ = final steady-state flow rate ($m^3/h$);
$Q_a$ = air flow rate ($m^3\,s^{-1}$);
$Q_w$ = water flow rate ($m^3\,s^{-1}$);
$R$ = hydraulic radius (m);
Re = Reynolds number;
$S_f$ = friction slope;
$T_s$ = preissmann slot width (m);
$t$ = time (s);
$U_w$ = average water velocity ($m\,s^{-1}$);
$Y$ = expansion factor;
$\Delta t$ = time step (s);
$\Delta x$ = space step (m);
$\rho_a$ = air density ($kg\,m^{-3}$);
$\rho_w$ = water density ($kg\,m^{-3}$); and
$\forall_a$ = air volume ($m^3$).

## Supplemental Materials

Figs. S1–S8 are available online in the ASCE Library (www.ascelibrary.org).

## References

AGA (American Gas Association). 1978. *Orifice metering of natural gas*. American National Standards Institute ANSI/API2530. New York: AGA.

Andey, S. P., and P. S. Kelkar. 2007. "Performance of water distribution systems during intermittent versus continuous water supply." *Am. Water Works Assoc.* 99 (8): 99–106. https://doi.org/10.1002/j.1551-8833.2007.tb08011.x.

Aureli, F., S. Dazzi, A. Maranzoni, and P. Mignosa. 2015. "Validation of single- and two-equation models for transient mixed flows: A laboratory test case." *J. Hydraul. Res.* 53 (4): 440–451. https://doi.org/10.1080/00221686.2015.1038324.

Binder, R. C. 1955. *Fluid mechanics*. 3rd ed. Hoboken, NJ: Prentice-Hall.

Cabrera, E., J. Abreu, R. Pérez, and A. Vela. 1992. "Influence of liquid length variation in hydraulic transients." *J. Hydraul. Eng.* 118 (12): 1639–1650. https://doi.org/10.1061/(ASCE)0733-9429(1992)118:12(1639).

Cabrera-Bejar, J. A., and V. G. Tzatchkov. 2009. "Inexpensive modeling of intermittent service water distribution networks." In *Proc., World Environmental and Water Resources Congress 2009*, 295–304. Reston, VA: ASCE. https://doi.org/10.1061/41036(342)29.

Campisano, A., A. Gullotta, and C. Modica. 2019. "Using EPA-SWMM to simulate intermittent water distribution systems." *Urban Water J.* 15 (10): 925–933. https://doi.org/10.1080/1573062X.2019.1597379.

Chaudhry, M. H. 2014. *Applied hydraulic transients*. 3rd ed. New York: Springer.

Christodoulou, S., and A. Agathokleous. 2012. "A study on the effects of intermittent water supply on the vulnerability of urban water distribution networks." *Water Supply* 12 (4): 523–530. https://doi.org/10.2166/ws.2012.025.

Ferreri, G. B., G. Freni, and P. Tomaselli. 2010. "Ability of Preissmann slot scheme to simulate smooth pressurisation transient in sewers." *Water Sci. Technol.* 62 (8): 1848–1858. https://doi.org/10.2166/wst.2010.360.

Fuertes-Miquel, V. S., O. E. Coronado-Hernández, D. Mora-Meliá, and P. L. Iglesias-Rey. 2019. "Hydraulic modeling during filling and emptying processes in pressurized pipelines: A literature review." *Urban Water J.* 16 (4): 299–311. https://doi.org/10.1080/1573062X.2019.1669188.

Guizani, M., J. Vasconcelos, S. J. Wright, and K. Maalel. 2006. "Investigation of rapid filling of empty pipes." *J. Water Manage. Model.* 14 (Jan): 463–482. https://doi.org/10.14796/JWMM.R225-20.

Gullotta, A., D. Butler, A. Campisano, E. Creaco, R. Farmani, and C. Modica. 2021. "Optimal location of valves to improve equity in intermittent water distribution systems." *J. Water Resour. Plann. Manage.* 147 (5): 04021016. https://doi.org/10.1061/(ASCE)WR.1943-5452.0001370.

Liou, C. P., and W. A. Hunt. 1996. "Filling of pipelines with undulating elevation profiles." *J. Hydraul. Eng.* 122 (10): 534–539. https://doi.org/10.1061/(ASCE)0733-9429(1996)122:10(534).

Malekpour, A., and B. Karney. 2014a. "Column separation and rejoinder during rapid pipeline filling induced by a partial flow blockage." *J. Hydraul. Res.* 52 (5): 693–704. https://doi.org/10.1080/00221686.2014.905502.

Malekpour, A., and B. W. Karney. 2014b. "Profile-induced column separation and rejoining during rapid pipeline filling." *J. Hydraul. Eng.* 140 (11): 1–12. https://doi.org/10.1061/(ASCE)HY.1943-7900.0000918.

Martin, C. S. 1976. "Entrapped air in pipelines." In *Proc., 2nd Int. Conf. on Pressure Surges*, 15–28. London: BHRA Fluid Engineering and City Univ.

Martins, N. M. C., J. N. Delgado, H. M. Ramos, and D. I. C. Covas. 2017. "Maximum transient pressures in a rapidly filling pipeline with entrapped air using a CFD model." *J. Hydraul. Res.* 55 (4): 506–519. https://doi.org/10.1080/00221686.2016.1275046.

Martins, S. C., H. M. Ramos, and A. B. Almeida. 2015. "Conceptual analogy for modelling entrapped air action in hydraulic systems." *J. Hydraul. Res.* 53 (5): 678–686. https://doi.org/10.1080/00221686.2015.1077353.

Pachaly, R., J. Vasconcelos, D. Allasia, and B. Minetto. 2019. "Field evaluation of discretized model setups for the storm water management model." *J. Water Manage. Model.* 27 (Apr): C463. https://doi.org/10.14796/JWMM.C463.

Pachaly, R. L., J. G. Vasconcelos, and D. G. Allasia. 2021a. "Surge predictions in a large stormwater tunnel system using SWMM." *Urban Water J.* 18 (8): 577–584. https://doi.org/10.1080/1573062X.2021.1916828.

Pachaly, R. L., J. G. Vasconcelos, D. G. Allasia, and J. P. P. Bocchi. 2021b. "Evaluating SWMM capabilities to simulate closed pipe transients." *J. Hydraul. Res.* 60 (1): 1–8. https://doi.org/10.1080/00221686.2020.1866695.

Pachaly, R. L., J. G. Vasconcelos, D. G. Allasia, R. Tassi, and J. P. P. Bocchi. 2020. "Comparing SWMM 5.1 calculation alternatives to represent unsteady stormwater sewer flows." *J. Hydraul. Eng.* 146 (7): 1–16. https://doi.org/10.1061/(ASCE)HY.1943-7900.0001762.

Pothof, I., and F. Clemens. 2010. "On elongated air pockets in downward sloping pipes." *J. Hydraul. Res.* 48 (4): 499–503. https://doi.org/10.1080/00221686.2010.491651.

Roesner, L. A., J. A. Aldrich, R. E. Dickinson, and T. O. Barnwell. 1988. *Storm water management model user's manual, Version 4: EXTRAN Addendum*. Washington, DC: Environmental Research Laboratory, Office of Research and Development, USEPA.

Romero, G., V. S. Fuertes-Miquel, Ó. E. Coronado-Hernández, R. Ponz-Carcelén, and F. Biel-Sanchis. 2020. "Analysis of hydraulic transients during pipeline filling processes with air valves in large-scale installations." *Urban Water J.* 17 (6): 568–575. https://doi.org/10.1080/1573062X.2020.1800762.

Rossman, L. A. 2017. *Storm water management model reference manual Volume II—Hydraulics*. Rep. No. EPA/600/R-17/111. Cincinnati: National Risk Management Laboratory, Office of Research and Development, USEPA.

Sharma, S. K., and K. Vairavamoorthy. 2009. "Urban water demand management: Prospects and challenges for the developing countries." *Water Environ. J.* 23 (3): 210–218. https://doi.org/10.1111/j.1747-6593.2008.00134.x.

Simukonda, K., R. Farmani, and D. Butler. 2018. "Intermittent water supply systems: Causal factors, problems and solution options." *Urban Water J.* 15 (5): 488–500. https://doi.org/10.1080/1573062X.2018.1483522.

Sjöberg, A. 1982. "Sewer network models DAGVL-A and DAGVL-DIFF." In *Urban stormwater hydraulics and hydrology*, 127–136. Littleton, CO: Water Resources Publ.

Stephenson, D. 1997. "Effects of air valves and pipework on water hammer pressures." *J. Transp. Eng.* 123 (2): 101–106. https://doi.org/10.1061/(ASCE)0733-947X(1997)123:2(101).

Vasconcelos, J., Y. Eldayih, Y. Zhao, and J. A. Jamily. 2018. "Evaluating storm water management model accuracy in conditions of mixed flows." *J. Water Manage. Model.* 27 (Jul): C451. https://doi.org/10.14796/JWMM.C451.

Vasconcelos, J. G., and D. T. Marwell. 2011. "Innovative simulation of unsteady low-pressure flows in water mains." *J. Hydraul. Eng.* 137 (11): 1490–1499. https://doi.org/10.1061/(ASCE)HY.1943-7900.0000440.

Zhou, F., F. E. Hicks, and P. M. Steffler. 2002. "Transient flow in a rapidly filling horizontal pipe containing trapped air." *J. Hydraul. Eng.* 128 (6): 625–634. https://doi.org/10.1061/(ASCE)0733-9429(2002)128:6(625).

Zhou, L., D. Liu, and B. Karney. 2013a. "Investigation of hydraulic transients of two entrapped air pockets in a water pipeline." *J. Hydraul. Eng.* 139 (9): 949–959. https://doi.org/10.1061/(ASCE)HY.1943-7900.0000750.

Zhou, L., D. Liu, B. Karney, and P. Wang. 2013b. "Phenomenon of white mist in pipelines rapidly filling with water with entrapped air pockets." *J. Hydraul. Eng.* 139 (10): 1041–1051. https://doi.org/10.1061/(ASCE)HY.1943-7900.0000765.

Zhou, L., D. Liu, B. Karney, and Q. Zhang. 2011. "Influence of entrapped air pockets on hydraulic transients in water pipelines." *J. Hydraul. Eng.* 137 (12): 1686–1692. https://doi.org/10.1061/(ASCE)HY.1943-7900.0000460.

Zhou, L., H. Wang, B. Karney, D. Liu, P. Wang, and S. Guo. 2018. "Dynamic behavior of entrapped air pocket in a water filling pipeline." *J. Hydraul. Eng.* 144 (8): 04018045. https://doi.org/10.1061/(ASCE)HY.1943-7900.0001491.